# Kernel Designs for Efficient Multiresolution Edge Detection and Orientation Estimation

R. Wilson, A.H. Bhalerao
Computer Science Department
University of Warwick
Coventry CV4 7AL
U.K.

21 May 1990

**Abstract**

This paper deals with the design of filter kernels having specified radial and angular frequency responses, based on combined optimization and frequency sampling. This is used to generate small radius lowpass and edge detection kernels for multiresolution pyramids. The performance of the new kernels in estimating orientation is shown to be significantly better than that of other commonly used pyramid kernels.

# 1 Introduction

Multiresolution or pyramidal techniques of image processing and analysis have played an increasingly important role in recent years, with applications ranging from enhancement [1] and data compression [2], [3] to edge detection [4] [5] [6] [7], texture analysis [8] and segmentation [9], [10]. The reason for these developments is the realisation that such methods provide a computationally efficient way to combine information from different scales. In the last few years, more emphasis has been placed on the relation of these techniques to linear transformations, such as the Gabor representation [11], the Wavelet transform [12] and the Multiresolution Fourier transform [13], which have an explicit representation of frequency and are often most efficiently computed using Fast Fourier Transform methods.

Nonetheless, there are still many applications where a pyramid based on lowpass filtering and decimation is an effective and simple representation. In particular, the perennial problem of detecting and representing localised image features such as edges is one which is easily accomplished using a lowpass pyramid and simple edge filters. While the Laplacian pyramid [2] is simple, it does not readily lend itself to computation of an essential edge parameter, orientation, due to the more or less circular symmetry of the operators involved. Moreover, if orientation is to be estimated, then a lowpass kernel which is more nearly circular than the Gaussian approximation of [2] is desirable. Similarly, the simpler edge operators described in the literature (*eg* [14]), while generally capable of some form of gradient direction estimate, are also biased in orientation. On the other hand, operators which have been designed specifically for orientation estimation are generally rather large in diameter and therefore expensive computationally [15] [16] [17] [18].

It is the purpose of this paper to describe designs for small radius kernels, both lowpass and edge filters, which are aimed at producing accurate orientation estimates with minimal computational demands. The filter kernels are produced using a combination of frequency sampling and optimization. They are shown to offer significantly improved estimation performance over other widely used kernels [2] [19] on test data, at little or no extra computational cost.

The next section of the paper contains a description of the design method. This is followed by the test results and discussion of possible extensions of the design method to other problems.

# 2 Kernel Designs

The design of two dimensional filter kernels is one of the oldest subjects in image processing, extending over the last twenty years [20] [21] [22] [19]. Although a number of techniques for obtaining circularly symmetric kernels have been described (*eg* [21] [22]), it remains true that many of the most widely used kernels are cartesian separable : they can be written in the form

$$h(x,y) = h_x(x)h_y(y) \tag{1}$$

Although in bygone days the speed premium implied by a reduction of the 2-d computation to two 1-d computations was important, this benefit is marginal in pyramid operations, due to subsampling, and so this restriction has been dropped, as it is particularly inappropriate for kernels whose response should be polar separable.

Of existing design methods, the two most widely used are functional minimization (or minimax) and frequency sampling (*eg* [21]). The method described below is a combination of the two, in which frequency sampling is used to constrain the rotational properties of the filter, while its radial response is specified as a minimization. The principal reason for this choice is that the rotational symmetries of the filter are thereby used as a constraint, rather than a component of the overall objective function. If the latter approach were adopted, the problem of assessing the relative importance of errors in radial response against those in angle would arise. In effect, by adopting the right form of frequency sampling, the filter is constrained to have a polar separable frequency response of the

form

$$H(\rho,\theta) = H_\rho(\rho)H_\theta(\theta) \tag{2}$$

where $\rho$ is the radial frequency and $\theta$ the angular frequency. As Knutsson [15] and Danielsson [17] have pointed out, such forms are necessary for the measurement of orientation. A further benefit is that it reduces the remaining optimization to one which is effectively 1-d, as is implied by the separation of variables in eqn(2). While not necessary, this simplification is nonetheless welcome.

Choice of the optimization criterion for the radial response is very much application dependent. While minimax methods [21] have an obvious attraction in applications with discrete or peaky spectra, the broad and essentially continuous spectrum of edge features suggests that a minimization of the average error such as least squares is more appropriate in the present application. Such a method was used successfully by Knutsson in the design of orientation estimation kernels [15] and also underlies the use of various forms of prolate spheroidal sequence in image filtering [8], [22].

Thus the radial component of the lowpass filter kernels is an approximation to the ideal 1-d lowpass filter, with a cut-off at $\pi/2$ radians, assuming 2:1 subsampling in each spatial dimension between successive pyramid levels [2],

$$H_\rho(\rho) = \begin{cases} 1 & \text{if } 0 \le \rho \le \pi/2 \\ 0 & \text{else} \end{cases} \tag{3}$$

The optimization problem is then of the form of a minimization of the weighted squared error

$$\min_{\alpha_k, 1\le k\le n} \int_{-\pi}^{\pi}\int_{0}^{R} \rho w(\rho)|H_\rho(\rho) - \hat{H}(\rho,\theta,\boldsymbol{\alpha})|^2 d\rho d\theta \tag{4}$$

where $\alpha_k$ are the spatial kernel coefficients, arranged in the vector $\boldsymbol{\alpha}$, so that

$$\hat{H}(\rho,\theta,\boldsymbol{\alpha}) = \sum_{k=1}^{n} \alpha_k \exp(-j\rho(x_k\cos\theta + y_k\sin\theta)) \tag{5}$$

where $(x_k, y_k)$ are the spatial coordinates of the kth coefficient. In eqn(4), the function $w(\rho)$ is a weighting function, which should reflect the relative importance of errors as a function of radial frequency. Now, there are two sources of error in this application : broadband noise and aliasing. Both will be emphasised by the edge detection, which is essentially a differentiation. It is therefore appropriate to use a weighting function which is increasing with radial frequency, such as the quadratic

$$w(\rho) = \rho^2 \tag{6}$$

The upper limit on radial frequency, R, was set at $\sqrt{2}\pi$, so that the area of integration covers the square representing one period of the necessarily periodic frequency response of the filter.

Now consider the form of the filter frequency response. There are two cases to consider. When n is odd, the filter is spatially symmetric about the origin and so its frequency response is the even function

$$\hat{H}(\rho,\theta,\boldsymbol{\alpha}) = \alpha_0 + 2\sum_{k=1}^{m} \alpha_k \cos(\rho(x_k\cos\theta + y_k\sin\theta)) \tag{7}$$

where $\alpha_0$ is the coefficient at $(0,0)$, $m = (n-1)/2$ and $x_k$ and $y_k$ are integer. For n even, the spatial symmetry is about a point midway between 4 sample points and so the response has the form

$$\hat{H}(\rho,\theta,\boldsymbol{\alpha}) = 2\exp(-j\rho(\cos\theta + \sin\theta)/2)\sum_{k=1}^{m} \alpha_k \cos(\rho(x_k\cos\theta + y_k\sin\theta)) \tag{8}$$

where $n = 2m$ and $x_k$ and $y_k$ are odd half-integers. Since the phase factor in eqn(8) is a simple consequence of the position of the kernel centre being midway between 4 sample points, it can be removed to give the real response

$$\hat{H}(\rho,\theta,\boldsymbol{\alpha}) = 2\sum_{k=1}^{m} \alpha_k \cos(\rho(x_k\cos\theta + y_k\sin\theta)) \tag{9}$$

The responses of eqns(7),(9) reflect the desired symmetry of the response to rotation by $\pi : (x_k, y_k) \rightarrow (-x_k, -y_k)$. While a further reduction is possible by symmetrization with respect to rotation by $\pi/2$, it is convenient to subsume this under the general symmetry requirement. Performing the implied differentiation on (4) yields

$$\int_{-\pi}^{\pi}\int_{0}^{R} \rho^3 \frac{\partial \hat{H}}{\partial \alpha_i}(H_\rho(\rho) - \hat{H}(\rho,\theta,\boldsymbol{\alpha}))d\rho d\theta = 0 \tag{10}$$

where

$$\frac{\partial \hat{H}}{\partial \alpha_i} = \begin{cases} 1 & \text{if } i = 0, n = 2m+1 \\ 2\cos(\rho(x_i\cos\theta + y_i\sin\theta)) & \text{else} \end{cases} \tag{11}$$

and substituting from eqns(3),(11) into (10) gives, for $n = 2m+1, i = 0$,

$$\int_{-\pi}^{\pi}\int_{0}^{\pi/2} \rho^3 d\rho d\theta = \int_{-\pi}^{\pi}\int_{0}^{R} \rho^3(\alpha_0 + 2\sum_{k=1}^{m} \alpha_k \cos(\rho(x_k\cos\theta + y_k\sin\theta)))d\rho d\theta \tag{12}$$

and for $i \neq 0$

$$\begin{aligned} &\int_{-\pi}^{\pi}\int_{0}^{\pi/2} \rho^3 \cos(\rho(x_k\cos\theta + y_k\sin\theta))d\rho d\theta = \\ &\quad \int_{-\pi}^{\pi}\int_{0}^{R} \rho^3[\alpha_0 \cos(\rho(x_i\cos\theta + y_i\sin\theta)) \\ &\quad +2\sum_{k=1}^{m} \alpha_k \cos(\rho(x_i\cos\theta + y_i\sin\theta))\cos(\rho(x_k\cos\theta + y_k\sin\theta))]d\rho d\theta \end{aligned} \tag{13}$$

while for $n = 2m$

$$\begin{aligned} &\int_{-\pi}^{\pi}\int_{0}^{\pi/2} \rho^3 \cos(\rho(x_i\cos\theta + y_i\sin\theta))d\rho d\theta = \\ &\quad 2\sum_{k=1}^{m} \alpha_k \int_{-\pi}^{\pi}\int_{0}^{R} \rho^3 \cos(\rho(x_i\cos\theta + y_i\sin\theta))\cos(\rho(x_k\cos\theta + y_k\sin\theta))d\rho d\theta \end{aligned} \tag{14}$$

After integration and simplification, eqns(12)-(14) reduce respectively to eqns(15)-(17), giving for $n = 2m+1$

$$\alpha_0 = 1/64 - 8\sum_{j=1}^{m} \alpha_j I(\sqrt{2}\pi r_j) \tag{15}$$

$$I(\pi r_i/2) - I(\sqrt{2}\pi r_i) = 64\sum_{j=1}^{m} \alpha_j [I(\sqrt{2}\pi s_{ij}) + I(\sqrt{2}\pi d_{ij}) - 8I(\sqrt{2}\pi r_i)I(\sqrt{2}\pi r_j)] \tag{16}$$

and, for $n = 2m$,

$$I(\pi r_i/2) = 64\sum_{j=1}^{m} \alpha_j [I(\sqrt{2}\pi s_{ij}) + I(\sqrt{2}\pi d_{ij})] \tag{17}$$

where

$$\begin{aligned} r_i^2 &= x_i^2 + y_i^2 \\ s_{ij}^2 &= (x_i + x_j)^2 + (y_i + y_j)^2 \\ d_{ij}^2 &= (x_i - x_j)^2 + (y_i - y_j)^2 \end{aligned} \tag{18}$$

and

$$I(r) = \begin{cases} 1/4 & \text{if } r = 0 \\ 1/r[J_1(r)(1 - 4/r^2) + 2/rJ_0(r)] & \text{if } r \neq 0 \end{cases} \tag{19}$$

$J_n(r)$ is the nth order Bessel function of the first kind [23]. Inspection of eqns(15),(16) shows that, for n odd, the centre coefficient is a linear combination of the remaining m coefficients, which are obtained by solution of a system of linear equations. For n even, a similar equation system results (eqn(17)). Thus, as might be expected, the filter kernel is defined by a linear system of the form

$$\boldsymbol{\beta} = \boldsymbol{B}\boldsymbol{\alpha} \tag{20}$$

where the scalars $\beta_i$ are given by the l.h.s. of eqns(16),(17) and the coefficient $B_{ij}$ is the coefficient multiplying $\alpha_j$ on the corresponding r.h.s..

Now, the addition of rotational symmetry constraints is achieved by demanding that the frequency response of the filter satisfies (*cf* eqn(7))

$$\hat{H}(\rho_i, \theta_i, \boldsymbol{\alpha}) = \hat{H}(\rho_i, 0, \boldsymbol{\alpha}) \quad 1 \leq i \leq n_1 \tag{21}$$

where

$$n_1 = \sqrt{n}(\sqrt{n} - 1)/2 \tag{22}$$

and the points $(\rho_i \cos\theta_i, \rho_i \sin\theta_i)$ are spaced on a cartesian lattice in the frequency plane, such that

$$\rho_i \cos\theta_i = rx_i \quad \rho_i \sin\theta_i = ry_i \tag{23}$$

and the constant $r > 0$ is selected so that the lattice covers the passband of the filter. This choice of frequency samples is convenient computationally because it preserves the natural rotational symmetries of the filter and has been found to give a frequency response which is very close to having circular symmetry. Since there are $n_1$ constraint equations, the number of degrees of freedom left for the minimization is reduced from $m$ to $(m - n_1)$.

The frequency sampling constraints can be expressed in the form of a linear system

$$\boldsymbol{C}\boldsymbol{\alpha} = \mathbf{o} \tag{24}$$

where the $(n_1 \times m)$ matrix $\mathbf{C}$ expresses the equalities of eqn(21). This set of linear equations can be recast, to give expressions for the coefficients $\alpha_i$ in terms of the $(m - n_1)$ components along the horizontal axis, $a_j$, say,

$$\boldsymbol{\alpha} = \boldsymbol{\Gamma}\boldsymbol{a} \tag{25}$$

where $\boldsymbol{\Gamma}$ is $(m \times (m - n_1))$. Substitution into eqn(20) then gives the equation set

$$\boldsymbol{\Gamma}^t\boldsymbol{B}\boldsymbol{\Gamma}\boldsymbol{a} = \boldsymbol{\Gamma}^t\boldsymbol{\beta} \tag{26}$$

In this way, the frequency sampling constraints, which ensure circular symmetry, reduce the size of the linear problem resulting from the optimization to $(m - n_1)$, effectively a reduction from a 2-d problem to a 1-d one.

This method has been used to design lowpass kernels of sizes $(4 \times 4)$ to $(6 \times 6)$. These are listed in Tables 1- 3.

The filters' frequency responses are shown on a dB scale in Figs 1- 3, along with the Gaussian kernel used by Burt and Adelson [2], Fig 4. The new $(5 \times 5)$ and $(6 \times 6)$ kernels are clearly superior to the Gaussian kernel, both in terms of stopband attenuation and circularity, while the new $(4 \times 4)$ kernel is roughly comparable in performance to the Gaussian one. It is perhaps worth mentioning as an aside that the kernels of even sizes are naturally preferable if a quadtree decimation is employed, while the $(5 \times 5)$ kernels fit the decimation scheme used by Burt and Adelson.

The second problem is the design of kernels for edge detection and orientation estimation. A number of authors have noted that the obvious method is to use a pair of approximations to partial derivatives in perpendicular directions for this task (*eg* [24], [25]). Indeed, the $(2 \times 2)$ Roberts operators are the oldest and simplest choice for this task [14]. Moreover, since they have only two nonzero coefficients, they have no spare degrees of freedom and so the design problem is non-existent. At the other end of the scale of complexity, the set of four quadrature filter pairs used by Knutsson [15] represents something of a gold standard in terms of accuracy, but is relatively expensive computationally. Since computational efficiency is one of the main concerns in the present work, it seems appropriate to attempt to generalise the Roberts kernels to produce $(3 \times 3)$ and $(4 \times 4)$ edge kernels with minimal estimation bias.

Now, for such small kernels, the number of degrees of freedom available to the designer is severely limited by the natural symmetries of the kernel. In the $(3 \times 3)$ case, there is only one degree of freedom governing the shape of the response and in the $(4 \times 4)$ only three. For this reason, there is little point in attempting both frequency sampling and optimization. Since for orientation estimation it is the angular response of the filter that is important, it was decided to use only frequency sampling to give an ideal response to 1-d image features, that is features with a frequency spectrum which is concentrated along a line at orientation $\theta_0$ [15], [25]

$$F(\rho, \theta) = 1/\rho F(\rho)\delta(\theta - \theta_0) \tag{27}$$

The edge detector frequency response can be expressed in the form

$$E(\rho, \theta) = 2j \sum_{k=1}^{m} \epsilon_k \sin(\rho(x_k \cos\theta + y_k \sin\theta)) \tag{28}$$

where $\epsilon_k$ is the $k$th spatial coefficient and where, as in eqn(9), the phase shift associated with even sized kernels is ignored. Taking $F(\rho)$ to be flat out to radial frequency $\pi$

$$F(\rho) = \begin{cases} 1 & \text{if } 0 \leq \rho \leq \pi \\ 0 & \text{else} \end{cases} \tag{29}$$

then gives the frequency sampling equations at angles $\theta_i$, based on the ideal (sinusoidal) response [25]

$$\int_0^{\pi} E(\rho, \theta_i) d\rho = j \sin(\theta_i + \pi/4) \tag{30}$$

which, after substitution from eqn(28) and integration, gives

$$2 \sum_{k=1}^{m} \epsilon_k I_1(x_k \cos\theta_i + y_k \sin\theta_i) = \sin(\theta_i + \pi/4) \tag{31}$$

where

$$I_1(r) = \begin{cases} 0 & r = 0 \\ 1/r(1 - \cos(\pi r)) & \text{else} \end{cases} \tag{32}$$

Solution of these equations for a suitably symmetric set of angles $\theta_i$ gave the edge kernels of Tables 4,5. The other kernel of each pair is obviously produced by a rotation of $\pi/2$.

The frequency responses of the new edge kernels are shown in Figs 5- 7 , where they can be compared with that of the Roberts kernels. The average deviation from a circular function is of the order of 2% for the $(3 \times 3)$ kernels and less than 1% for the $(4 \times 4)$ kernels. It seems doubtful whether an increase in size over the $(4 \times 4)$ would be repaid in terms of reduced error.

# 3 Test Results

Since a major aim of the present work was to give accurate estimates of the orientations of image features, both the test pattern and the error criterion have been chosen to reflect that aim.

The choice of test pattern for comparing the filters was motivated by the desire to have a broad range of frequencies and all orientations, with approximately equal energies in each frequency band. The result is a circular, frequency modulated pattern, which is similar to that used by Knutsson [15], but in which the wavelength increases linearly from 4 pixels to 64 pixels from the outer rim of the pattern to its inner rim. The result is that roughly equal areas are devoted to all spatial frequencies in the band. The image is of size $(256 \times 256)$. The test used both a clean test pattern and one corrupted by additive white Gaussian noise, having a signal-noise ratio of 15dB. Fig. 8 shows the lowpass pyramids obtained from the test pattern using the $(6 \times 6)$ kernel in comparison with the 'optimal' kernel of Meer et al [19]. The lack of circular symmetry and relatively high level of aliasing are quite visible in the Meer kernel, which has traded off these defects for uniformity of response in the passband.

The error criterion was based on the 'double-angle' representation of orientation introduced by Granlund and Knutsson [15, 16]. This representation, which is best explained in terms of the inertia ellipse defined by the distribution of signal energy in the Fourier domain [24], takes account of the Hermitian symmetry of the Fourier transform. In the present case, if the two edge detector outputs are written in polar form as

$$\begin{aligned} g_1(x,y) &= r(x,y)\cos\theta(x,y) \\ g_2(x,y) &= r(x,y)\sin\theta(x,y) \end{aligned} \tag{33}$$

then the double-angle vector representation is given by

$$t_2(x,y) = \begin{pmatrix} 2r^2(x,y)\cos\theta(x,y)\sin\theta(x,y) \\ r^2(x,y)(\cos^2\theta(x,y) - \sin^2\theta(x,y)) \end{pmatrix} \tag{34}$$

Unlike the conventional gradient, whose components are just $g_i(x,y), i = 1,2$, this representation has the advantage of being independent of the input signal phase, an important property when the test pattern is locally sinusoidal. It also has some attractions in a number of applications [15]. The results show the output signal-noise ratio based on the known orientation of each point in the test pattern and that estimated as in eqn(34), ie the double-angle

$$\Phi = \sum_{(x,y)} r(x,y)\cos(Arg[t_2(x,y)] - 2Arg[(x,y)])/\sum_{(x,y)} r(x,y) \tag{35}$$

In effect, $\Phi$ is the correlation between the estimated vectors $t_2(x,y)$ and the 'ideal' vectors, which have unit magnitude and orientation $2Arg[(x,y)]$. The signal-noise ratio is then defined to be

$$SNR = 10\log_{10}\frac{\Phi}{1-\Phi} \tag{36}$$

To give an idea of scale, a 1 deg. error in angle corresponds to a SNR of 32dB. The graphs show the SNR as a function of pyramid level for various combinations of lowpass and edge kernels. The results presented in Figs 9- 12 show the relative performances of the new lowpass kernels and the Gaussian and Meer kernels in construction of lowpass pyramids, from which the orientations were estimated using the $(2 \times 2)$ Roberts edge detectors, for the clean test image (Fig 9) and the noisy one (Fig 10). In Figs 11 and 12, the pyramids obtained from the two test images using the $(5 \times 5)$ lowpass kernel were used as input to the three sizes of edge detector kernels and the best $(3 \times 3)$ edge kernels reported in the literature [17]. The results show the importance of good lowpass kernel design in the estimation of orientation and demonstrate that the edge kernel design method is effective. Overall,

there is a significant improvement using the new kernels - more than 6dB on average, for the $(6 \times 6)$ kernel, compared with the Gaussian kernel . From the clean input image, the results show that aliasing has been greatly reduced for the new $(5 \times 5)$ and $(6 \times 6)$ kernels, as intended. It should also be noted that above level 1 of the pyramid, there is little change in the output SNR. This is because the smoothing affects both signal and errors equally - the test image has a broad spectrum.

In summary, it can be claimed that the new kernels do offer significant performance improvement in terms of the accuracy of orientation estimates for a given computational cost.

# 4 Conclusions

It has been shown that the filter designs presented in this paper offer a real improvement in performance over commonly used kernels in orientation estimation, with comparable computational cost. The design technique used to obtain them is simple and reasonably flexible - it could be applied to other problems requiring a specified angular response and desired radial response, such as anisotropic enhancement and segmentation [1], [26], [27]. The well known limitations of frequency sampling need to be borne in mind when considering such developments, however (*eg* [21]). Filters requiring more complex angular behaviour than can be expressed in the first few circular harmonic functions are probably better synthesized using straightforward optimization methods. Nonetheless, to the extent that a given radial and angular response can be reasonably approximated by small radius kernels, the method presented here is effective.

One issue which has not been addressed so far in this work is that of spatial localisation and the resulting "uncertainty principle" conflict between spatial and frequency domain properties, about which much has been written in recent years [8], [11]. This simply reflects the fact that the spatial locality of the filters' impulse responses is automatically constrained by their spatial support. In this respect, the new lowpass kernels are closely related to the prolate spheroidal sequences - they are spatially finite, but have as much energy as possible inside of the radial passband $(0 \leq \rho \leq \pi/2)$. Where they differ is in the weighting of the deviation from an ideal response : for prolate spheroidal sequences, the weighting is uniform, but for these filters it increases with frequency. In effect, this trades off uniformity of response in the passband for increased stopband attenuation. Whether this is desirable depends on the application - in the applications where an invertible image description is desired, uniformity of response is arguably more important [8], [13].

# Acknowledgement

This work was supported in part by U.K. SERC. The authors wish to express their appreciation to Shell Research Ltd. for their financial support. They are indebted to Dr. S Graham of Shell Research Ltd., Sittingbourne Research Centre, for his encouragement and valued discussions on the work.

# References

[1] S. C. Clippingdale and R. Wilson, "Least Squares Estimation on a Multiresolution Pyramid," in *Proc. ICASSP-89*, (Glasgow), pp. 1409–12, 1989.

[2] P. J. Burt and E. H. Adelson, "The Laplacian Pyramid as a Compact Image Code," *IEEE Trans. Comp.*, vol. COM-31, pp. 532–540, 1983.

[3] M. Todd and R. Wilson, "An Anisotropic Multiresolution Image Data Compression Algorithm," in *Proc. ICASSP-89*, (Glasgow), pp. 1969–72, 1989.

[4] A. Rosenfeld and M. Thurston, "Edge and Curve Detection for Visual Scene Analysis," *IEEE Trans. Comp.*, vol. 5, no. 20, pp. 562–569, 1971.

[5] A. P. Witkin, "Scale-Space Filtering," in *Proc. IJCAI*, (Karlsruhe), 1983.

[6] F. Bergholm, "Edge Focusing," *IEEE Trans. P.A.M.I.*, vol. 9, no. 6, pp. 726–741, 1987.

[7] A. Schrift, Y. Y. Zeevi, and M. Porat, "The Most Significant Edges: an Efficient Image Description for Machine Vision Applications," in *Proc. IAPR Workshop on Comp. Vis.*, (Tokyo), pp. 340–2, 1988.

[8] R. Wilson and M. Spann, "Finite Prolate Spheroidial Sequence and Their Applications I, II: Image Feature Description and Segmentation," *IEEE Trans. P.A.M.I.*, vol. 10, pp. 193–203, 1988.

[9] P. J. Burt, T. H. Hong, and A. Rosenfeld, "Segmentation and Estimation of Image Region Properties Through Cooperative Hierarchical Computation," *IEEE Trans. Sys, Man Cyber.*, vol. 11, no. 12, pp. 802–809, 1981.

[10] M. Spann and R. G. Wilson, "A Quad-Tree Approach to Image Segmentation Which Combines Statistical and Spatial Information," *Pattern Recognition*, vol. 18, no. 3/4, pp. 257–269, 1985.

[11] J. G. Daugman, "Complete Discrete 2-d Gabor Transforms by Neural Networks for Image Analysis and Compression," *IEEE Trans. Acous. Speech Sig. Proc.*, vol. 36, pp. 1169–79, 1988.

[12] S. G. Mallat, "A Theory for Multiresolution Signal Decomposition: the Wavelet Representation," *IEEE Trans. P.A.M.I.*, vol. 11, pp. 674–93, 1989.

[13] A. Calway and R. G. Wilson, "A Unified Approach to Feature Extraction Based on an Invertible Image Transform," in *Proc. 3rd IEE Int. Conf. Image Processing*, (Warwick, U.K), pp. 651–655, 1989.

[14] R. C. Gonzalez and P. Wintz, *Digital Image Processing (2nd. Ed).* Addison-Wesley, New York, 1987.

[15] H. Knutsson, *Filtering and Reconstruction in Image Processing.* PhD thesis, University of Linköping, Sweden, 1982.

[16] H. E. Knutsson, R. Wilson, and G. H. Granlund, "Estimation the Local Orientation of Anisotropic 2-d Signals," in *Proc. IEEE ASSP Workshop on Spect. Est.*, (Tampa), pp. 234–9, 1983.

[17] P. E. Danielsson, "Rotation-Invariant Linear Operators with Directional Response," in *Proc. 5th ICPR*, (Miami), pp. 1171–6, 1980.

[18] R. Lenz, "Optimal Filters for the Detection of Linear Patterns in 2-d Higher Dimensional Images," *Pattern Recognition*, vol. 20, pp. 163–72, 1987.

[19] P. Meer, E. S. Baugher, and A. Rosenfeld, "Frequency Domain Analysis and Synthesis of Pyramid Generating Kernels," *IEEE Trans. P.A.M.I.*, vol. 9, pp. 512–22, 1987.

[20] T. S. Huang, "Two-dimensional Windows," *IEEE Trans. Audio Electroacous.*, vol. 20, pp. 88–9, 1972.

[21] L. R. Rabiner and B. Gold, *Theroy and Applications of Digital Signal Processing.* Prentice Hall, Englewood-Cliffs, 1975.

[22] R. Chapman and T. S. Durrani, "Circularly Symmetric Filter Design Using 2-d Prolate Spheroidial Sequences," in *Proc. ICASSP-84*, (San Diego), pp. 20.3.1–4, 1984.

[23] G. N. Watson, *A Treatise on the Theory of Bessel Functions (2nd ed.).* Cambridge University Press, Cambridge, 1958.

[24] J. Bigun, *Local Symmetry Features in Image Processing.* PhD thesis, University of Linköping, Sweden, 1988.

[25] P. E. Danielsson and O. Seeger, "Rotation Invariance in Gradient and Higher Order Derivative Operators," *Comp. Vision Graphics and Im. Proc.*, vol. 49, pp. 198–221, 1990.

[26] R. Wilson, S. C. Clippingdale, and A. H. Bhalerao, "Robust Estimation of Local Orientations in Images Using a Multiresolution Approach," in *Proc. 5rd SPIE Conf. Vis. Comm. Image Proc.*, (Lausanne), 1990.

[27] A. Bhalerao and R. G. Wilson, "Multiresolution Image Segmentation Combining Region and Boundary Information," Tech. Rep. RR154, Department of Computer Science, University Of Warwick, Coventry, U.K., 1989.

| | | | |
|---|---|---|---|
| .0109 | .0582 | .0582 | .0109 |
| .0582 | .1227 | .1227 | .0582 |
| .0582 | .1227 | .1227 | .0582 |
| .0109 | .0582 | .0582 | .0109 |

Table 1: $(4 \times 4)$ filter kernel

| | | | | |
|---|---|---|---|---|
| .0006 | .0178 | .0290 | .0178 | .0006 |
| .0178 | .0670 | .0880 | .0670 | .0178 |
| .0290 | .0880 | .1194 | .0880 | .0290 |
| .0178 | .0670 | .0880 | .0670 | .0178 |
| .0006 | .0178 | .0290 | .0178 | .0006 |

Table 2: $(5 \times 5)$ filter kernel

| | | | | | |
|---|---|---|---|---|---|
| 0 | .0040 | .0117 | .0117 | .0040 | 0 |
| .0040 | .0266 | .0507 | .0507 | .0266 | .0040 |
| .0117 | .0507 | .0906 | .0906 | .0507 | .0117 |
| .0117 | .0507 | .0906 | .0906 | .0507 | .0117 |
| .0040 | .0266 | .0507 | .0507 | .0266 | .0040 |
| 0 | .0040 | .0117 | .0117 | .0040 | 0 |

Table 3: $(6 \times 6)$ filter kernel

| | | |
|---|---|---|
| -.0741 | -.0955 | 0 |
| -.0955 | 0 | .0955 |
| 0 | .0955 | .0741 |

Table 4: $(3 \times 3)$ edge kernel

| | | | |
|---|---|---|---|
| -.0107 | -.0469 | -.0277 | 0 |
| -.0496 | -.1292 | 0 | .0277 |
| -.0277 | 0 | .1292 | .0496 |
| 0 | .0277 | .0496 | .0170 |

Table 5: $(4 \times 4)$ edge kernel

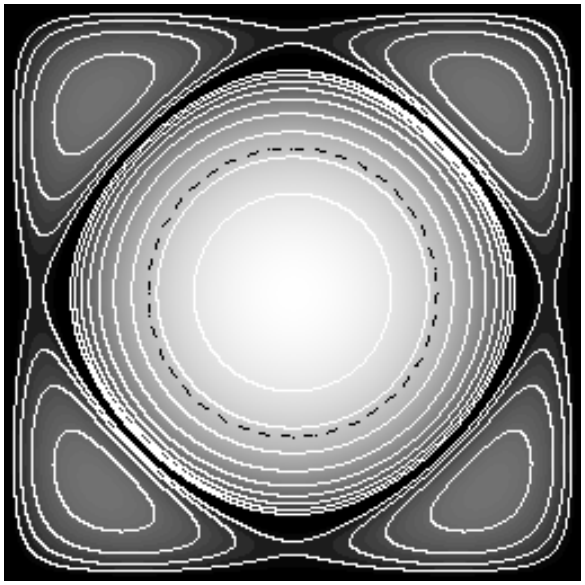

Figure 1: Frequency response of optimised lowpass size (4x4). White lines showing 10db contours with $\pi/2$ cut-off shown by black dashed circle

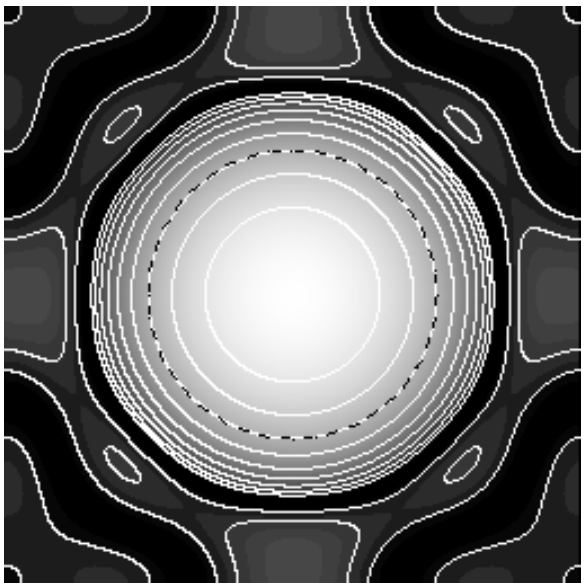

Figure 2: Frequency response of optimised lowpass size (5x5)

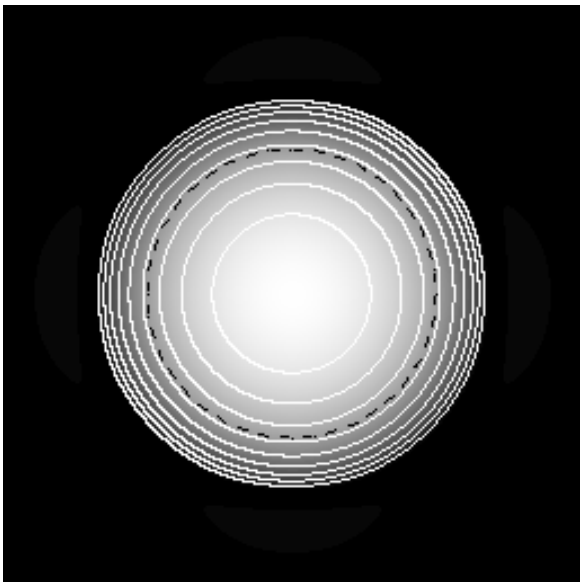

Figure 3: Frequency response of optimised lowpass size (6x6)

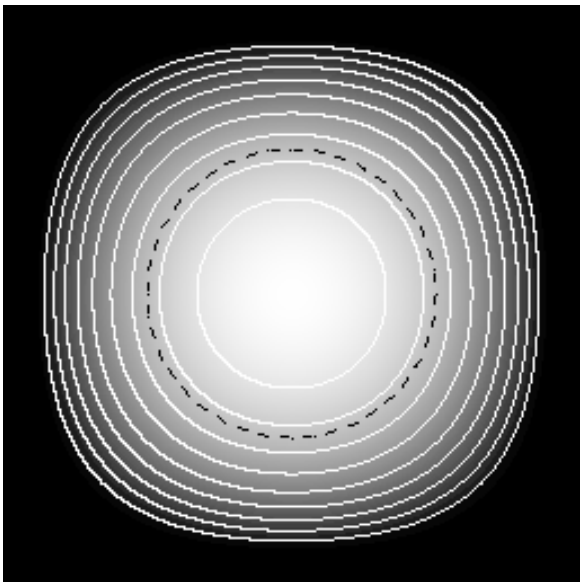

Figure 4: Frequency response of Burt-Adelson Gaussian kernel size (5x5)

Figure 5: Frequency response of Roberts edge kernel (2x2). White lines showing 10db contours

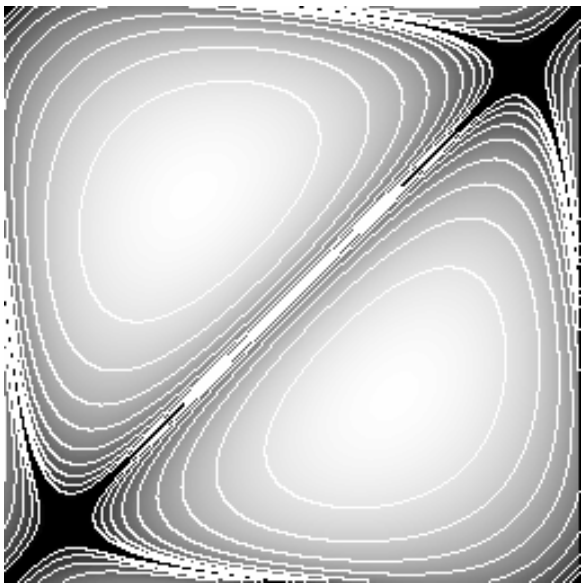

Figure 6: Frequency response of optimised edge kernel (3x3)

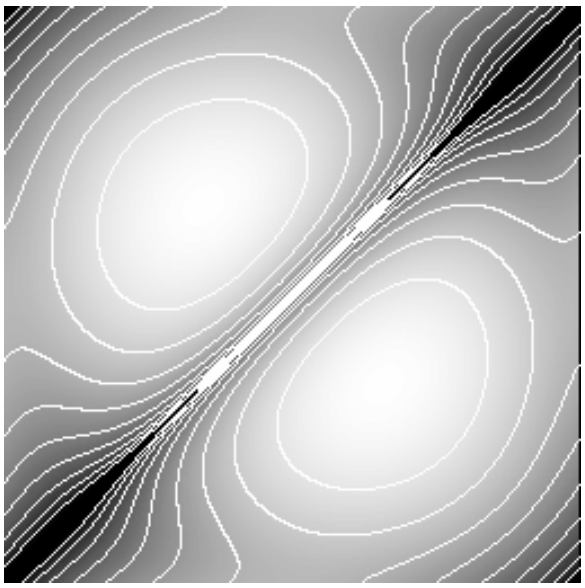

Figure 7: Frequency response of optimised edge kernel (4x4)

Figure 8: Pyramids of linear FM test pattern using optimised lowpass kernel size 6x6 (top) and Meer *et al* size 13x13 (bottom)

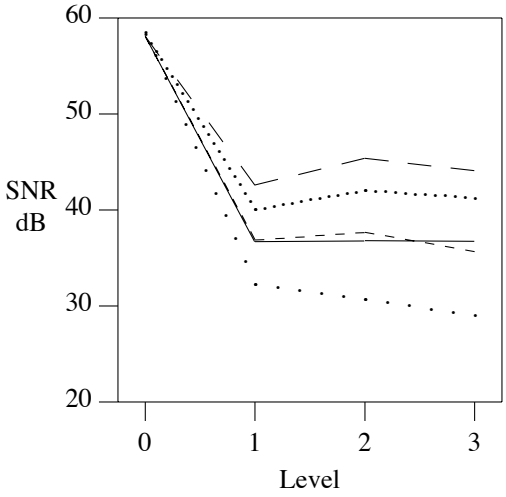


Figure 9: SNR comparing low pass pyramid kernels: Burt-Adelson 5x5 (—), Meer *et al* 13x13 (. . .), Optimised: 4x4 (- -), 5x5 (···), 6x6 (– –)

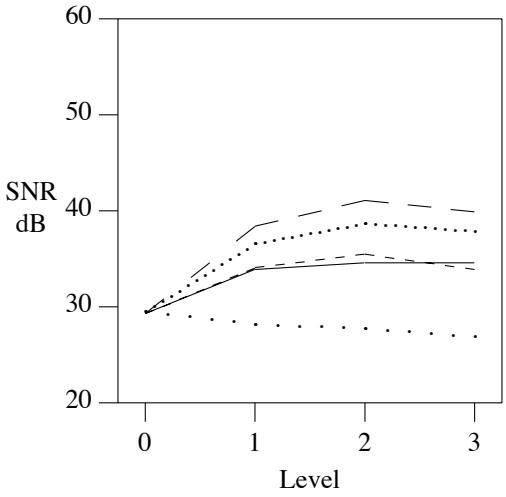


Figure 10: SNR comparing low pass pyramid kernels on 15dB data

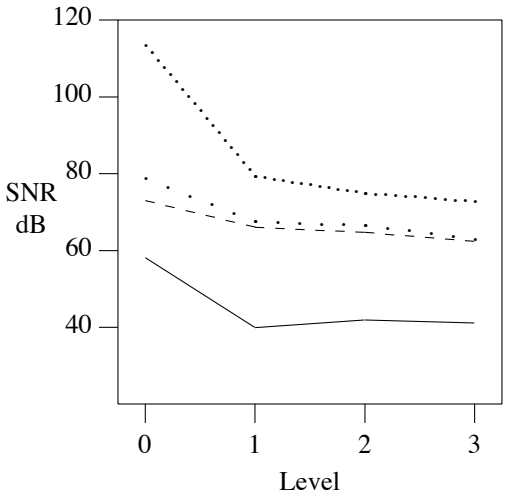


Figure 11: SNR comparing edge kernels: Roberts 2x2 (—), Danielsson-Seeger Sobel 3x3 (. . .), Optimised: 3x3 (- -), 4x4 (···)

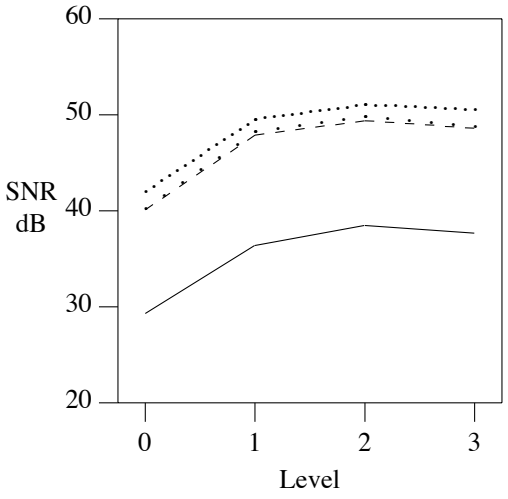


Figure 12: SNR comparing edge kernels on 15dB data